Strategy for solving difficulties in spin-glass simulations

Tota Nakamura

Faculty of Engineering, Shibaura Institute of Technology, 307 Fukasaku, Minuma, Saitama 337-8570, Japan

A spin-glass transition has been investigated for a long time but we have not reached a conclusion yet due to difficulties in the simulation studies. They are slow dynamics, strong finite-size effects, and sample-to-sample dependencies. We found that a size of the spin-glass order reaches a lattice boundary within a very short Monte Carlo step. A competition between the spin-glass order and a boundary condition causes these difficulties. Once the boundary effect was removed, physical quantities exhibited quite normal behaviors. They became self-averaging in a limit of large replica numbers. These findings suggest that the nonequilibrium relaxation method is a good choice for solving the difficulties if a lattice size and a replica number are set sufficiently large. A dynamic scaling analysis on nonequilibrium relaxation functions gave a result that the spin-glass transition and the chiral-glass transition occurs at the same temperature in the Heisenberg model in three dimensions. The estimated critical exponent ν agrees with the experimental result.

I. INTRODUCTION

A spin glass (SG) [1–5] is a random magnet consisting of ferromagnetic interactions and antiferromagnetic interactions distributed randomly. It shares common interest and difficulties with other random systems. A spin-glass study has been a challenging field of developing an efficient numerical algorithm. One successful achievement is the temperature-exchange method [6]. It is now a standard algorithm in SG simulations and applied to various complex systems. A quantum-annealing algorithm [7] was also developed to obtain the ground state of the SG system. It is considered as a practical solution for various nonconvex optimization problems.

In this paper, we focus on a problem whether the SG transition in the Heisenberg model is driven by the spin degrees of freedom or the chirality degrees of freedom. The Heisenberg SG model is the first approximation for the canonical SG materials. An origin of the debate on this model dates back to a work by Olive, Young, and Sherrington [8], where the SG transition was not observed by the Monte Carlo (MC) simulations. The simulations were performed up to a linear lattice size $L = 32$. Kawamura [5,9] introduced the chirality scenario, wherein the SG transition observed in real materials was considered as an outcome of the chiral-glass (CG) transition without the SG transition. A finite spin anisotropy was considered to mix the SG order and the CG order. Its counterargument is an existence of a simultaneous SG and CG transition, which was observed by MC simulations [10–20]. However, the results supporting the chirality scenario were also reported at the same time [21–23]. Two studies [24–26] in both sides drew two opposite conclusions even though the authors performed similar amounts of simulations, but treated the finite-size effects differently. The linear sizes were $L = 8$–48 [24] and $L = 6$–32 [25,26]. A strong finite-size effect hopelessly prevented us to reach a conclusion. This situation motivated this paper.

Previous simulation studies mostly applied the equilibrium MC method and the finite-size scaling analysis. The simulations suffer from severe slow dynamics: it takes a very long time to equilibrate the system. We also need to take averages of physical quantities over different realizations of random bond configurations. A sufficient sample number increases when there are strong sample-to-sample dependencies. Then, a more computational time is needed, and we can simulate only small-lattice systems. The obtained data include strong finite-size effects. A finite-size scaling analysis encounters large finite-size corrections. Then, a disagreement mentioned above may occur even though acceleration algorithms were developed and used. These are common difficulties in random systems.

In order to solve the difficulties in SG simulations, we need to reexamine this strategy. In this paper, we clarified that an origin of the difficulties is a boundary effect. A strategy based on the nonequilibrium relaxation method [27–29] was shown to be very efficient. This method studies a phase transition through relaxation functions of physical quantities. We run a simulation on a very large system and stop the simulation before the finite-size effect appears. The obtained relaxation functions are free from the finite-size effect. We can determine the critical temperature and critical exponents by the dynamic scaling analysis on the relaxation functions. Therefore, this method has been successfully applied [13,20,30–39] to spin glasses and other systems with frustration and randomness. Other successful dynamical approaches to the spin-glass transition were also reported [40,41].

This paper is organized as follows. Section II describes the model we treat in this paper. We also give expressions for observed physical quantities. In Sec. III, we clarify an origin of the simulation difficulties. In Sec. IV, we introduce our strategy. In Sec. V, numerical results are presented. Section VI is devoted to summary and discussions.

II. MODEL AND OBSERVABLES

A Hamiltonian of the present model is written as follows:

$$\mathcal{H} = -\sum_{\langle ij \rangle} J_{ij} \boldsymbol{S}_i \cdot \boldsymbol{S}_j. \qquad (1)$$

The sum runs over all the nearest-neighbor spin pairs $\langle ij \rangle$. The interactions J_{ij} take Gaussian variables with a zero mean and a standard deviation J. The temperature T is scaled by J. Linear lattice size is denoted by L. A total number of spins is $N = L \times (L-1)^2$, and skewed periodic boundary conditions are imposed.

We calculated in our simulations the SG and the CG susceptibility χ_{SG} and χ_{CG}, and the SG and the CG correlation functions f_{SG} and f_{CG}, from which we estimated the SG and the CG correlation lengths ξ_{SG} and ξ_{CG}. We evaluated these quantities at MC steps t, with a same interval in a logarithmic scale, namely, at $t = 10^{0.05i}$ with an integer i.

The SG susceptibility is defined by the following expression:

$$\chi_{SG} \equiv \frac{1}{N} \left[\sum_{i,j} \langle \boldsymbol{S}_i \cdot \boldsymbol{S}_j \rangle^2 \right]_c. \qquad (2)$$

The thermal average is denoted by $\langle \dots \rangle$, and the random-bond configurational average is denoted by $[\dots]_c$. The thermal average is replaced by an average over independent real replicas that consist of different thermal ensembles:

$$\langle \boldsymbol{S}_i \cdot \boldsymbol{S}_j \rangle = \frac{1}{m} \sum_{A=1}^{m} \boldsymbol{S}_i^{(A)} \cdot \boldsymbol{S}_j^{(A)}. \qquad (3)$$

The superscript A is a replica index. A replica number is denoted by m. We prepare m real replicas for each random-bond configuration with a different initial spin state. Each replica is updated using a different random number sequence. A replica number controls an accuracy of the thermal average.

An overlap between two replicas A and B is defined by

$$q_{\mu\nu}^{AB} \equiv \frac{1}{N} \sum_i S_{i\mu}^{(A)} S_{i\nu}^{(B)}. \qquad (4)$$

Here, subscripts μ and ν represent three components of Heisenberg spins: x, y, and z. The SG susceptibility is rewritten using this overlap as

$$\chi_{SG} = \frac{N}{C_m} \left[\sum_{A>B,\mu,\nu} \left(q_{\mu\nu}^{AB} \right)^2 \right]_c. \qquad (5)$$

Here, $C_m = m(m-1)/2$ is a combination number of choosing two replicas out of m replicas. Similarly, the CG susceptibility is defined by

$$\chi_{CG} \equiv \frac{3N}{C_m} \left[\sum_{A>B} \left(q_\kappa^{AB} \right)^2 \right]_c, \qquad (6)$$

where

$$q_\kappa^{AB} \equiv \frac{1}{3N} \sum_{i,\mu} \kappa_{i,\mu}^{(A)} \kappa_{i,\mu}^{(B)}, \qquad (7)$$

$$\kappa_{i,\mu}^{(A)} \equiv \boldsymbol{S}_{i+\hat{\boldsymbol{e}}_\mu}^{(A)} \cdot \left(\boldsymbol{S}_i^{(A)} \times \boldsymbol{S}_{i-\hat{\boldsymbol{e}}_\mu}^{(A)} \right). \qquad (8)$$

This $\kappa_{i,\mu}^{(A)}$ is a local scalar chirality, where $\hat{e}_\mu$ denotes a unit lattice vector along the μ axis.

An SG correlation function is defined by the following expressions:

$$f_{SG}(r) \equiv \left[\frac{1}{N} \sum_i^N \langle \boldsymbol{S}_i \cdot \boldsymbol{S}_{i+r} \rangle^2 \right]_c \qquad (9)$$

$$= \left[\frac{1}{NC_m} \sum_{A>B,i,\mu,\nu} q_{\mu\nu}^{AB}(i) q_{\mu\nu}^{AB}(i+r) \right]_c \qquad (10)$$

$$= \left[\frac{1}{N} \sum_i^N \left(\frac{1}{m} \sum_{A=1}^m \boldsymbol{S}_i^{(A)} \cdot \boldsymbol{S}_{i+r}^{(A)} \right)^2 \right]_c. \qquad (11)$$

Here, remind that a thermal average is replaced by an average over m real replicas as shown in Eq. (3). We did not exclude out terms of the same replica in the square of Eq. (11) in order to follow its definition (9). When a replica number is two, it is equivalent to the four-point correlation function as shown in Eq. (10). Since we will use a large replica number up to 72 in this study, it is very time consuming to take an average over C_m different overlap functions. Therefore, we took another expression (11). For a given distance r, we calculated a spin correlation function at a site i for each replica A, and store it in an array memory of i. Then, a replica average is taken and the value is squared. We can obtain the correlation function $f_{SG}(r)$ by taking an average of the squared value over lattice sites i. Changing a value of r with the same procedure, we finally evaluated all the correlation functions. A total calculation time is reduced by this procedure because the maximum value of $r = L/2 - 2$ is much smaller than C_m. Here, we considered the correlations for three directions, $(1,0,0)$, $(0,1,0)$, and $(0,0,1)$, and took an average over them. We obtained a CG correlation function in a same manner replacing the local spin variables with the local chirality variables:

$$f_{CG}(r) = \left[\frac{1}{3N} \sum_{i,\mu}^N \left(\frac{1}{m} \sum_A^m \kappa_{i,\mu}^{(A)} \kappa_{i+r,\mu}^{(A)} \right)^2 \right]_c. \qquad (12)$$

A unit of three neighboring spins in a same direction is considered and values for three directions are averaged.

In most simulation studies, a correlation length has been estimated using the second-moment method [42] $\xi = \sqrt{\chi_0/\chi_k - 1}/k$, where χ_0 denotes the susceptibility and χ_k denotes the Fourier transform of the susceptibility with the smallest wave number k. As a system size increases, χ_k approaches χ_0 and k approaches zero. Then, an estimated value of ξ includes a large statistical error by a situation of $0/0$. On the other hand, the value includes a systematic error, which is on the order of ξ/L, when a lattice size is small.

In this paper, we estimated the correlation length by the Bayesian inference [43] using the data of correlation functions. The Bayesian theorem exchanges a prior probability and a posterior probability. For example, let us suppose that a correct correlation length $\xi(t)$ was obtained at each MC step t. Because of the critical scaling hypothesis, the correlation function behaves as $r^{-d+2-\eta}$, where, d is a dimension and
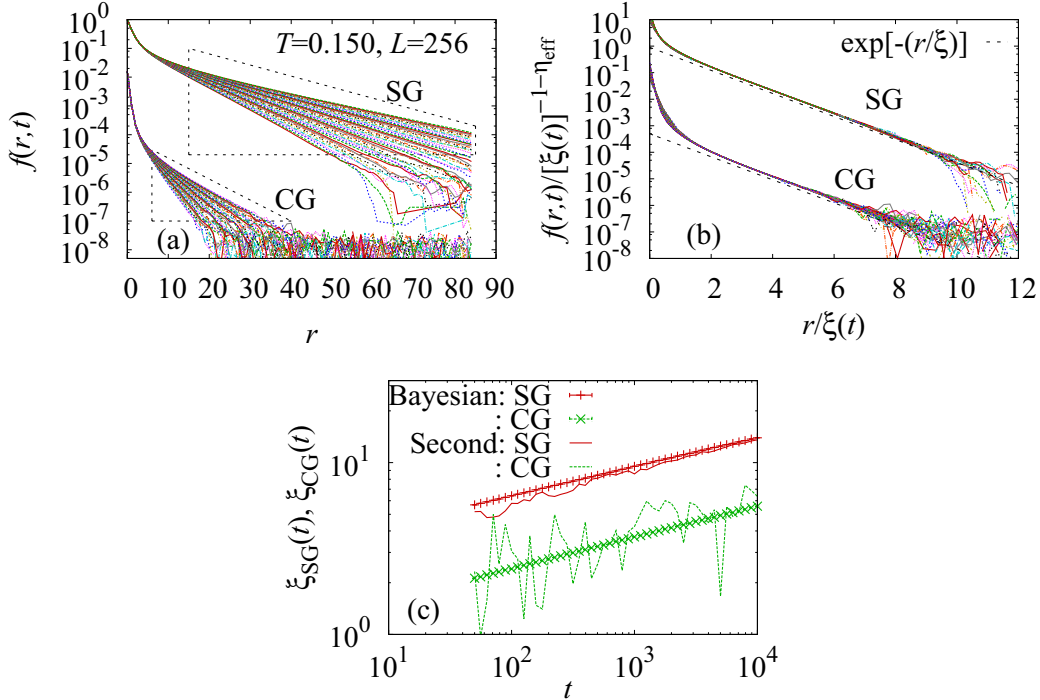
FIG. 1. (a) SG- and CG-correlation functions at time steps ranging from 50 to 10 000 when $T = 0.15$ and $L = 256$. Data within the dotted lines are used to estimate the correlation length. (b) A scaling plot of the correlation functions. Effective exponents are $\eta_{\text{eff}} = 0.221$ for SG and $\eta_{\text{eff}} = 0.593$ for CG. (c) Symbols with error bars depict estimated data of the correlation length. We also plotted with lines results obtained by the second-moment method.

$d = 3$ here. If we scale r by the correlation length $\xi(t)$, a correlation function at each step $f(r, t)$ is rescaled by $\xi^{-1-\eta}(t)$. Therefore, the correlation function data should be scaled by plotting $f(r, t)/\xi^{-1-\eta}(t)$ versus $r/\xi(t)$. The scaled function exhibits a single-exponential decay $\exp[-(r/\xi)]$ in a long-distance limit. Now, we use the Bayesian theorem and exchange the argument. Proper $\xi(t)$ and η_{eff} can be obtained as scaling parameters such that the scaling plot became the best under a condition that the scaled function exhibits a single-exponential decay as $\exp[-(r/\xi)]$ in a long-distance limit. This inference procedure is performed by the kernel method [44,45]. This is a machine learning algorithm, which automatically finds the parameters. We do not assume any form of the scaling function but just need to define an x coordinate and a y coordinate of plotted data. As for another approach for estimating the correlation length reducing the instability, Belletti *et al.* [46] proposed to obtain it by a ratio of integrals $I_k = \int r^k f(r) dr$.

Figure 1(a) shows data of the correlation functions. Each correlation function exhibits a single-exponential decay in a long-distance limit. In an inference procedure, we discarded data of short MC steps($t < 50$), data of short-range correlation ($r < 15$ for SG, and $r < 6$ for CG), data near the boundary ($r > L/3$), and data of small $f(r, t)$ values [$f(r, t) < 2 \times 10^{-5}$ for SG and $f(r, t) < 1 \times 10^{-7}$ for CG]. A result of the scaling is shown in Fig. 1(b). All the data ride on a single line: the correlation function mainly exhibits a single-exponential decay with its slope one. Each scaled function of f_{SG} deviated downward when it became below 10^{-4} suggesting a faster decay in a long-distance limit. This faster decay issue was discussed recently by Fernandez *et al.*

[47]. The estimated correlation-length data are plotted with symbols in Fig. 1(c). Error bars are negligible. We also plotted with lines results obtained by the second-moment method. The data fluctuate much and we cannot study the behavior of relaxation functions with them.

III. DIFFICULTIES IN SPIN-GLASS SIMULATIONS

A. Finite-size effects

We first check finite-size effects of χ_{SG} and χ_{CG}. Figure 2 shows the relaxation functions for lattice sizes from $L = 20$ to 256 at $T = 0.15$ and at $T = 0.17$. Both temperatures are located in the paramagnetic phase. Relaxation functions of lattice sizes larger than 40 at $T = 0.17$ exhibit size independence and realize at the final step an equilibrium state in the thermodynamic limit. When a size effect appeared, a relaxation function of χ_{SG} deviated to a lower side, and that of χ_{CG} deviated to an upper side. For example, this finite-size crossover of χ_{SG} occurred at $t \simeq 10$ when $L = 40$ at $T = 0.15$. However, it took 10^4 steps to reach the equilibrium state. Most of the time steps required for equilibration were spent after this size effect appeared. We also found that the equilibration time steps of χ_{SG} are always equal to those of χ_{CG} even though the finite-size crossover times are different. The SG order is waiting for the CG order to be equilibrated.

The finite-size effects of χ_{SG} and χ_{CG} are better understood by observing their profiles. A profile of the susceptibility is a correlation function $f(r)$ multiplied by $4\pi r^2$ plotted against r. An integration of this value with respect to r gives the susceptibility: $\chi = \int_0^{L/2} 4\pi r^2 f(r) dr$, when L is large enough.
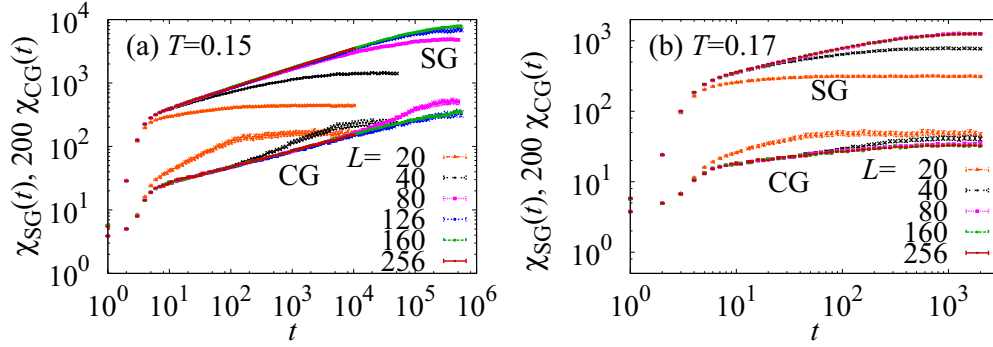
FIG. 2. Relaxation functions of χ_{SG} and χ_{CG} for various lattice sizes for (a) $T = 0.15$ and (b) $T = 0.17$. Data of χ_{CG} are multiplied by 200.

We find by this plot how each correlation function contributes to the susceptibility, and how large the ordered cluster is.

Figure 3(a) shows a profile of χ_{SG} at $t = 10$, 10^3, and 10^4 for various lattice sizes when $T = 0.15$. They correspond to relaxation functions of χ_{SG} in Fig. 2(a). A distance r at which the profile line reaches zero is regarded as a radius of the ordered cluster. Its diameter, $2r$, is a size of the cluster. The profiles exhibit a size-independent shape as long as a cluster size did not exceed a lattice size. The cluster size reached 60 even when $t = 10$. We checked that this short-time behavior is independent of the temperature. The finite-size crossover of χ_{SG} for $L = 40$ at $T = 0.15$ is explained by this profile. After the SG cluster size reached the boundary, the SG correlation connects with each other beyond the periodic boundary. The profile line is lifted due to this self-correlation. Finally, in the equilibrium state of small lattices, the profiles just exhibit monotonic increasing behaviors. On the other hand, a profile of a larger lattice exhibits a long tail converging slowly to zero. Therefore, the SG susceptibility is always very much underestimated when a lattice size is small. Figure 3(b) shows profiles of χ_{CG} in the same conditions as Fig. 3(a). A tail of profile drops rapidly even when a lattice size is large. There is an additional strong peak at $r = 1$. A strong finite-size enhancement causes a finite-size effect of χ_{CG} appearing as overestimating.

Figure 4 shows the scaled profiles at a time step when the correlation length reached each value ranging from 5 to 13 for SG and that ranging from 2 to 5 for CG. Since $\chi_{SG} \sim \xi_{SG}^{2-\eta}$, a profile of χ_{SG} is scaled by $\xi_{SG}^{1-\eta}$ if plotted against r/ξ_{SG}. Here, η is an effective exponent obtained by the correlation-function

scaling when we estimated the correlation length. We checked that a shape of the scaled profiles remains the same at each temperature if the cluster size is smaller than the lattice size no matter whether the system is in the nonequilibrium state or in the equilibrium state.

We found in these figures that the SG and CG profiles always reach zero when $r/\xi > 10$. We can guarantee that the finite-size effects do not appear if we set $L > 2r = 20\xi_{SG}$. This is a criterion of choosing lattice size and the simulation time range in this paper.

B. Sample dependencies

We must take averages of physical quantities over different random samples in SG simulations. Collected data are considered to depend on each sample. Before taking this sample average, we must take the thermal average. Then, there arises a question. Which number should be set large first, a replica number m or a sample number n_s?

Figure 5 shows the answer. We estimated a relative standard deviation of χ_{SG}, and plotted it against $1/\sqrt{m(m-1)/2}$. We changed a replica number from 2 to 72, and a sample number from 3 to 8. We also compared data free from the boundary effects and those affected by them. Figure 5(a) shows results at $T = 0.15$. Data free from the boundary effects were taken in the nonequilibrium process before the SG cluster size reached the lattice boundary. They rode on a straight line as a replica number increases, and converged to zero in a limit of $m \to \infty$. We also found that the relative errors are proportional to $1/\sqrt{m(m-1)/2}$ not to $1/\sqrt{m}$. This
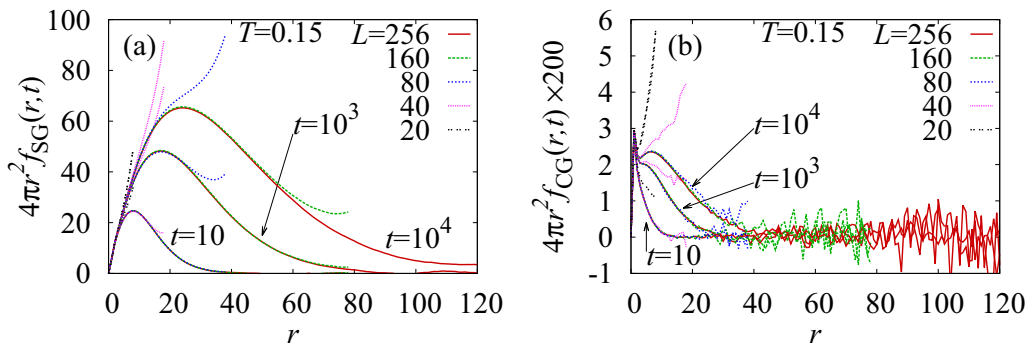

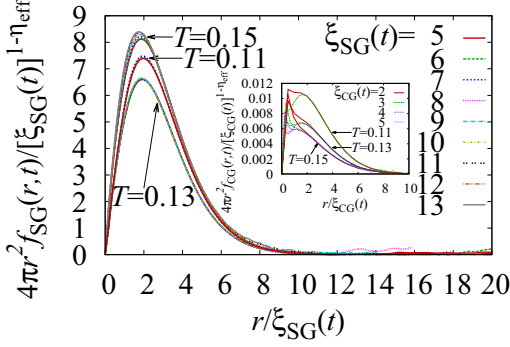FIG. 3. Profiles of χ_{SG}(a) and χ_{CG}(b) at $T = 0.15$.

FIG. 4. Profiles of scaled χ_{SG} plotted against r/ξ_{SG} when ξ_{SG} reached the denoted value ranging from 5 to 13. The effective exponents are $\eta_{\text{eff}} = -0.030$ for $T = 0.11$, $\eta_{\text{eff}} = -0.0087$ for $T = 0.13$, and $\eta_{\text{eff}} = 0.22$ for $T = 0.15$. Inset is a same plot for χ_{CG}. The effective exponents are $\eta_{\text{eff}} = 0.15$ for $T = 0.11$, $\eta_{\text{eff}} = 0.19$ for $T = 0.13$, and $\eta_{\text{eff}} = 0.59$ for $T = 0.15$. The linear lattice size is 256.

suggests that each replica *overlap* is independent, not that each replica is independent. Data affected by the boundary effects were taken in the nonequilibrium process after the SG cluster size reached the lattice boundary. They converged to a finite value.

Figure 5(b) shows data that were estimated after the equilibrium states were realized at $T = 0.17$. An equilibrium cluster size was roughly 200. Data of $L > 200$ are free from the boundary effect, and converged linearly to zero. Those of $L < 200$ converged to finite values, which decrease as L increases. Figure 5(c) shows data below the critical temperature. The SG

cluster size did not exceed the lattice size within the simulated time steps. They also converged linearly to zero. These data exhibit the same tendency. Therefore, data of each random sample are considered to be independent and *equivalent* in a limit of $m \to \infty$, if the profiles are free from the boundary effect no matter whether it is in the equilibrium state or in the nonequilibrium state, and also no matter whether the temperature is above or below the critical temperature.

Since the computational cost is proportional to $L^3 m n_s$, it is better to increase m first in order to reduce the numerical errors within a restricted computational time. In this paper, we set m to 64 or 72, and set n_s mostly to 4–8 when $L = 256$. We increased n_s up to 10 according to the sample fluctuations particularly near the critical temperature. A choice of a replica number larger than two has been applied in nonequilibrium relaxation analyses on the SG transition [13,30,34,36,37]. A reduction of statistical errors by increasing replica numbers was reported in Ref. [37] and recently analyzed in Ref. [48].

IV. OUR STRATEGY

Difficulties in SG simulations are strong finite-size effects, strong sample dependencies, and the slow dynamics. In the previous section, we found that a competition between the SG order and the boundary condition is the main origin of these difficulties. Therefore, we adopted the nonequilibrium relaxation method [27–29]. We do not need to solve a difficulty of slow dynamics, but we rather utilize it by analyzing the relaxation functions of physical quantities before the finite-size effects appeared. We remove the size effects by keeping a lattice size $L > 20\,\xi_{SG}$ and solve the sample dependence by increasing a replica number first.
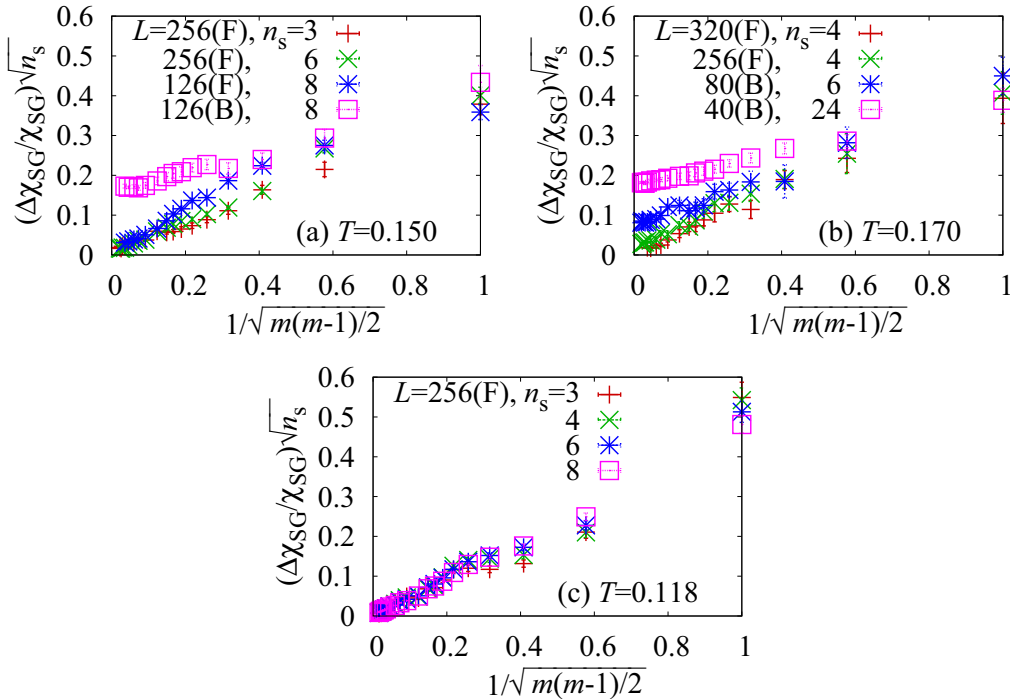

FIG. 5. Relative standard deviations of χ_{SG} are plotted against $1/\sqrt{m(m-1)/2}$ for various lattice sizes and sample numbers for (a) $T = 0.15$, (b) $T = 0.17$, and (c) $T = 0.118$. (F) stands for the data taken when the χ_{SG} profile was (F)ree from the boundary. (B) stands for the data taken after the χ_{SG} profile reached the (B)oundary.

We investigated the critical phenomena using the dynamic correlation-length scaling analysis [30]. This is a direct application of the scaling hypothesis,

$$\chi \sim \xi^{2-\eta}, \quad \xi \sim |T - T_c|^{-\nu}, \tag{13}$$

to the nonequilibrium relaxation data. The critical temperature is denoted by T_c in this expression. We replace ξ by its relaxation data $\xi(t_i, T_i)$, and replace χ by its relaxation data $\chi(t_i, T_i)$ in Eq. (13). Here, i denotes an index of data. We plot data with their coordinates (x_i, y_i) defined as

$$x_i = \xi(t_i, T_i)/|T_i - T_c|^{-\nu}, \quad y_i = \chi(t_i, T_i)/\xi^{2-\eta}(t_i, T_i). \tag{14}$$

Then, we estimate T_c, ν, and $2 - \eta$ so that all the data fall on a single curve. We can use data of temperatures both below and above the critical temperature because x_i is defined with an absolute value of the temperature difference. The parameter estimations were performed using the kernel method proposed by Harada [45]. It realizes unbiased and precise estimations of critical parameters without supposing any form of the scaling function.

Let us briefly explain the kernel method. We define a Gaussian kernel function $K(x_i, x_j)$ for $x_i \neq x_j$ as

$$K(x_i, x_j) = \theta_1^2 \exp\left[-\frac{(x_i - x_j)^2}{2\theta_2^2}\right] + \theta_3^2, \tag{15}$$

where θ_1, θ_2, and θ_3 are hyperparameters. A generalized covariance matrix Σ is defined as

$$\Sigma_{ij} = [\Delta(y_i)]^2 \delta_{ij} + K(x_i, x_j), \tag{16}$$

where $\Delta(y_i)$ denotes an error of y_i. Then, we define the following log-likelihood function, which should be maximized in regard to the scaling parameters and hyperparameters

$$\ln(\Lambda) = -\ln|\Sigma| - y_i \Sigma_{ij}^{-1} y_j, \tag{17}$$

where summations over i and j are taken. This log-likelihood function is defined independently for both above and below the critical temperature. Both estimates are divided by a number of data, and are taken average.

One advantage of the dynamic correlation-length scaling analysis is that both finite time t and finite size L do not appear explicitly in the scaling expression. We only deal with the physical quantities χ and ξ. Usually, a finite size and a finite time produce nontrivial effects in the SG system. Scaling analyses replacing ξ by size or time may need special attention to the scaling form we treat. Additional correction-to-scaling terms are sometimes necessary. Such nontrivial effects become hidden in the present correlation-length scaling analysis by plotting $\chi(t)$ against $\xi(t)$.

Let us summarize our simulation conditions here. MC simulations are performed by the single-spin-flip algorithm. One MC step consists of one heat-bath update, 124 overrelaxation updates, and 1/20 Metropolis update (once every 20 steps). We start simulations with random spin configurations. The temperature is quenched to a finite value at the first Monte Carlo step. The linear lattice size was fixed to 256. The temperature ranges from $T = 0.02$ to 0.18 at 73 different temperature points. Random bond configurations are generated independently at each temperature. The sample numbers are mostly 6, but we increased it up to 10 when

the data fluctuations were large. Total sample number for all the temperatures is 432. A replica number is mostly 72. We increased it to 88 at some temperatures in order to check if there are systematic dependencies on a replica number. In the scaling analysis, we discarded data at very low temperatures $T < 0.10$ because the scaled data separate from the data of $T \geqslant 0.10$. A typical initial step is 50, and a typical final step is 10 000. We increased it at most up to 31 623 at low temperatures. Only data with $\xi_{SG}(t) < L/20 = 12.8$ are used in the scaling analysis.

V. RESULTS

Figure 6(a) shows relaxation functions of χ_{SG} and χ_{CG} at typical temperatures. A slope of this figure corresponds to a ratio of critical exponents $(2 - \eta)/z = \gamma/z\nu$. It decreases with the temperature decreasing because of an increase of the dynamic exponent in the low-temperature phase. Figure 6(b) shows the corresponding relaxation functions of correlation lengths. A slope of this figure is an inverse of the dynamic exponent: $1/z$. We plotted $\chi(t)$ against $\xi(t)$ in Fig. 6(c). We found that there is no bending anomaly from the nonequilibrium relaxation process to the equilibrium relaxation process. This plot tells us that both processes smoothly connect with each other if we plot $\chi(t)$ against $\xi(t)$.

We obtained the critical temperature and the critical exponents by the dynamic correlation-length scaling analysis. There were 2816 data points of (ξ, χ) for different time steps and temperatures. We randomly selected 1400 data points out of them and applied the kernel method. We checked the obtained results by a cross validation method. Namely, we randomly reselected 1400 data points again and tested the obtained parameters by estimating a log-likelihood function. We tried this check for 10 times by changing the selected data and took an average of $-\ln(\Lambda)$ over them. Then, one estimated set of $(T_c, \nu, 2 - \eta)$ and $-\ln(\Lambda)$ are obtained. We repeated this trial for 100 times and took averages over results whose $-\ln(\Lambda)$ values only differ within the standard deviation from the best value. We put error bars by this standard deviation among these results.

Results of the trial are shown in Fig. 7. Figures 7(a)–7(c) show the $-\ln(\Lambda)$ plotted against the estimated critical temperature, the estimated ν, and the estimated $\gamma(= \nu \times (2 - \eta))$, respectively. An estimate is better if $-\ln(\Lambda)$ is lower. A rectangle shows the estimated error bar. Figure 7(d) shows relations between the estimated $2 - \eta$ and the estimated critical temperature. We also plotted with lines the effective $2 - \eta_{eff}$ obtained in the ξ estimation. It is expected to coincide with $2 - \eta$ at $T = T_c$. However, there are small differences between them.

Figure 8 shows the scaling plot using the estimated critical parameters

$$T_{SG} = 0.140 \pm 0.002 \, (0.1395), \tag{18}$$

$$\nu_{SG} = 1.41 \pm 0.10 \, (1.401), \tag{19}$$

$$2 - \eta_{SG} = 1.96 \pm 0.02 \, (1.967), \tag{20}$$
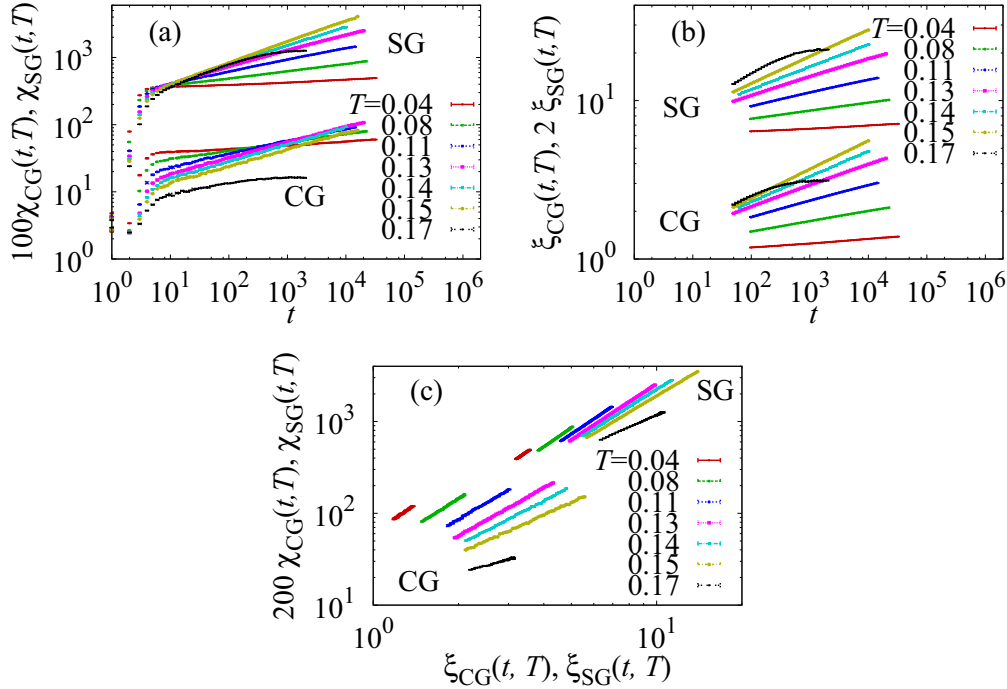
$$\gamma_{SG} = 2.76 \pm 0.22 \, (2.755), \tag{21}$$

FIG. 6. (a) Relaxation functions of χ_{SG} and χ_{CG}. Data of χ_{CG} are multiplied by 100 in order to fit in a same window. (b) Relaxation functions of ξ_{SG} and ξ_{CG}. Data of ξ_{SG} are multiplied by 2 in order to separate them from the ξ_{CG} data. (c) A cross plot of the susceptibility against the correlation length.

and

$$T_{CG} = 0.140 \pm 0.002 \, (0.1382), \tag{22}$$

$$\nu_{CG} = 1.61 \pm 0.09 \, (1.693), \tag{23}$$

$$2 - \eta_{CG} = 1.60 \pm 0.04 \, (1.637), \tag{24}$$

$$\gamma_{CG} = 2.59 \pm 0.20 \, (2.771). \tag{25}$$

A value in parentheses denotes the estimate that gave the best likelihood function. The SG critical temperature coincided with the CG one. This value disagrees with the one estimated by Fernandez *et al.* [24], who reported $T_{SG} = T_{CG} = 0.120$. It also disagrees with the one estimated by Viet and Kawamura [25], who reported $T_{SG} = 0.125$, but their value $T_{CG} = 0.143$ is close to our estimate. Some of their data before the size extrapolation are consistent with our result. The size extrapolation depends on the way how the correction-to-scaling terms are treated. There is no finite-size correction in the present analysis. A finite-time correction may exist and it

can be controlled using a standard finite-size scaling theory once if the time is connected with the length by the dynamic correlation-length data $\xi(t)$ [40,41]. We did not treat it in this paper but just discarded short-step data such that the scaling plot becomes excellent. A correlation length mostly ranges from 5 to 13 in our analyses. If a true critical phenomena was observed only beyond this length scale, the present results should be modified.

Let us study a behavior of the dynamic exponent z. Since $\xi(t) \sim t^{1/z}$ in the critical region, we can define an effective dynamic exponent $z_{\rm eff}$ by an inverse of a slope of Fig. 6(b) in the nonequilibrium process before the finite-size crossover occurred. We estimated the value by the least-square method. As shown in Fig. 9(a), the effective dynamic exponent of SG is always larger than that of CG. Our estimate at the transition temperature is $z_{SG} = 7.3(3)$ for SG and $z_{CG} = 6.4(2)$ for CG. A divergence of ξ_{SG} is slower than that of ξ_{CG}. On the other hand, a coupled exponent $z\nu$ took the same value as $z_{SG}\nu_{SG} = z_{CG}\nu_{CG} = 10.3$. This agreement means that a
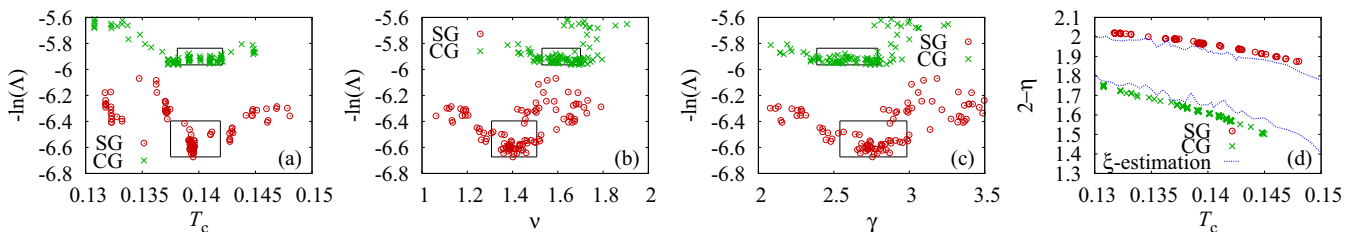

FIG. 7. (a)–(c) Likelihood functions plotted against the estimated parameters for each scaling trial. (d) Relation between the estimated $(2 - \eta)$ and the critical temperature. Effective $2 - \eta$ obtained in the ξ estimation is also plotted with line.
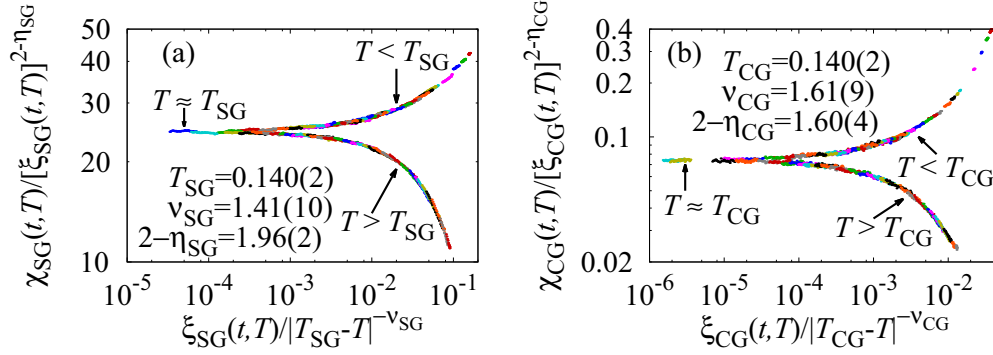
FIG. 8. Dynamic correlation-length scaling plots of χ_{SG}-ξ_{SG} (a) and χ_{CG}-ξ_{CG} (b) using Eq. (14). Data of $0.02 \leqslant T \leqslant 0.18$ are plotted.

correlation time of SG diverges with the same speed as that of CG because a correlation time $\tau \sim |T - T_c|^{-z\nu}$. The effective dynamic exponent rapidly increased below the critical temperature faster than a behavior of $1/z \propto T$, which was reported [49–53] previously. There is no anomaly down to the lowest temperature we simulated. This smooth behavior is consistent with the one reported [49] in the Ising SG model.

We also studied a temperature dependence of a coupled exponent $(2 - \eta)/z$, which is a slope of Fig. 6(a). The results are plotted in Fig. 9(b). This coupled exponent of SG and that of CG behave in a same manner down to the lowest temperature. The values at the critical temperature were 0.266(10) for SG and 0.257(16) for CG. This agreement means that dynamics of χ_{SG} is equivalent to that of χ_{CG} because $\chi(t) \sim t^{(2-\eta)/z}$.

VI. SUMMARY AND DISCUSSION

We found that the finite-size effect is a main origin of the difficulties in SG simulations. As was observed in the SG profile, the cluster size is very large even at a considerably short step. It reached 60 lattice spacings only at $t = 10$ as shown in Fig. 3(a). This initial relaxation behavior was temperature independent. We may easily encounter this finite-size effect in SG simulations.

A relaxation process after the finite-size effect appeared is much longer than the one before it. The equilibrium simulation must overcome this long relaxation process but the nonequilibrium simulation does not need to. This is the reason for an advantage of the nonequilibrium relaxation method.

A sample deviation of the SG susceptibility also vanished linearly with $1/m \to 0$ when the finite-size effect did not appear. We observed these evidences regardless of whether they are nonequilibrium ones or equilibrium ones, and regardless of whether the temperature is above or below the critical temperature. Therefore, an elimination of the finite-size effect was the first approach to solve the difficulties in SG simulation.

The boundary-affected equilibrium state that hit the boundary within the initial relaxation process may not include a relevant information. Therefore, we sometimes encounter a size crossover only above which the data should be used to study the critical phenomena. This size crossover was first observed by Hukushima and Campbell [54] who reported it in the Ising SG model. The correlation-length ratio changed its trend from increasing to decreasing at a crossover size $L = 24$.

We confirmed that the SG transition and the CG transition occur at the same temperature within the error bars. A critical exponent γ took a common value, but other critical exponents ν, $2 - \eta$, and z were different between them. However, if we coupled exponents as $z\nu$ and $(2 - \eta)/z$, they took common values between SG and CG. It suggests that critical phenomena of spin glasses are better understood by these coupled exponents. We compared our results with the previous works in Table I. A value of ν_{SG} is common between the Gaussian model and the $\pm J$ model. It is also consistent with a value of ν_{CG}. Even if a spin anisotropy effect mixes the spin degrees of freedom and the chirality degrees of freedom, a value of ν may not change much. Therefore, our estimate was also consistent
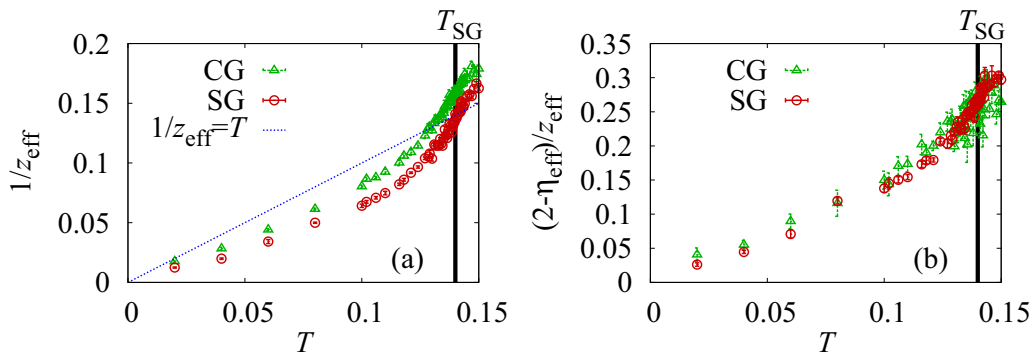

FIG. 9. Temperature dependencies of effective exponents (a) $1/z_{eff}$ and (b) $(2 - \eta_{eff})/z_{eff}$.

TABLE I. Comparison of present results with the previous works. (G) stands for the Gaussian bond distribution model, (J) stands for the $\pm J$ bond distribution model, and (Ex) stands for experimental results.

Works	T_{SG}	T_{CG}	ν_{SG}	ν_{CG}	η_{SG}	η_{CG}
Present (G)	0.140(2)	0.140(2)	1.4(1)	1.6(1)	0.04(2)	0.40(4)
Ref. [24] (G)	0.120(6)	0.120(6)	1.5	1.4(1)	−0.15(5)	−0.75(15)
Ref. [25] (G)	0.125(6)	0.143(3)		1.4(2)		0.6(2)
Ref. [23] (J)	0	0.19(1)		1.3(2)		0.8(2)
Ref. [43] (J)	0.203(1)	0.201(1)	1.49(3)	1.53(3)	0.28(1)	0.66(1)
Ref. [55] (Ex)			1.3–1.4		0.4–0.5	

with the experimental result [55]. On the other hand, a value of η depends much on the distribution and on each analysis. The SG values and the CG value also differ much. We cannot conclude which one can explain the experimental result.

[1] K. Binder and A. P. Young, Rev. Mod. Phys. **58**, 801 (1986).

[2] J. A. Mydosh, *Spin Glasses* (Taylor & Francis, London, 1993).

[3] *Spin Glasses and Random Fields*, edited by A. P. Young (World Scientific, Singapore, 1997).

[4] N. Kawashima and H. Rieger, in *Frustrated Spin Systems*, edited by H. T. Diep (World Scientific, Singapore, 2004).

[5] H. Kawamura, J. Phys. Soc. Jpn. **79**, 011007 (2010).

[6] K. Hukushima and K. Nemoto, J. Phys. Soc. Jpn. **65**, 1604 (1996).

[7] T. Kadowaki and H. Nishimori, Phys. Rev. E **58**, 5355 (1998).

[8] J. A. Olive, A. P. Young, and D. Sherrington, Phys. Rev. B **34**, 6341 (1986).

[9] H. Kawamura, Phys. Rev. Lett. **68**, 3785 (1992).

[10] F. Matsubara, S. Endoh, and T. Shirakura, J. Phys. Soc. Jpn. **69**, 1927 (2000).

[11] S. Endoh, F. Matsubara, and T. Shirakura, J. Phys. Soc. Jpn. **70**, 1543 (2001).

[12] F. Matsubara, T. Shirakura, and S. Endoh, Phys. Rev. B **64**, 092412 (2001).

[13] T. Nakamura and S. Endoh, J. Phys. Soc. Jpn. **71**, 2113 (2002).

[14] L. W. Lee and A. P. Young, Phys. Rev. Lett. **90**, 227203 (2003).

[15] L. Berthier and A. P. Young, Phys. Rev. B **69**, 184423 (2004).

[16] M. Picco and F. Ritort, Phys. Rev. B **71**, 100406(R) (2005).

[17] I. Campos, M. Cotallo-Aban, V. Martin-Mayor, S. Perez-Gaviro, and A. Tarancón, Phys. Rev. Lett. **97**, 217204 (2006).

[18] L. W. Lee and A. P. Young, Phys. Rev. B **76**, 024405 (2007).

[19] T. Shirakura and F. Matsubara, J. Phys. Soc. Jpn. **79**, 075001 (2010).

[20] T. Nakamura and T. Shirakura, J. Phys. Soc. Jpn. **84**, 013701 (2015).

[21] K. Hukushima and H. Kawamura, Phys. Rev. E **61**, R1008 (2000).

[22] M. Matsumoto, K. Hukushima, and H. Takayama, Phys. Rev. B **66**, 104404 (2002).

[23] K. Hukushima and H. Kawamura, Phys. Rev. B **72**, 144416 (2005).

[24] L. A. Fernandez, V. Martin-Mayor, S. Perez-Gaviro, A. Tarancon, and A. P. Young, Phys. Rev. B **80**, 024422 (2009).

[25] D. X. Viet and H. Kawamura, Phys. Rev. Lett. **102**, 027202 (2009).

[26] D. X. Viet and H. Kawamura, Phys. Rev. B **80**, 064418 (2009).

[27] D. Stauffer, Phys. A (Amsterdam) **186**, 197 (1992).

[28] N. Ito, Phys. A (Amsterdam) **192**, 604 (1993).

[29] Y. Ozeki and N. Ito, J. Phys. A: Math. Gen. **40**, R149 (2007).

[30] T. Nakamura, Phys. Rev. B **82**, 014427 (2010).

[31] Y. Ozeki and N. Ito, Phys. Rev. B **64**, 024416 (2001).

[32] Y. Ozeki and N. Ito, Phys. Rev. B **68**, 054414 (2003).

[33] T. Shirahata and T. Nakamura, Phys. Rev. B **65**, 024402 (2001).

[34] T. Nakamura, S. Endoh, and T. Yamamoto, J. Phys. A: Math. Gen. **36**, 10895 (2003).

[35] T. Shirahata and T. Nakamura, J. Phys. Soc. Jpn. **73**, 254 (2004).

[36] T. Yamamoto, T. Sugashima, and T. Nakamura, Phys. Rev. B **70**, 184417 (2004).

[37] T. Nakamura, arXiv:cond-mat/0603062.

[38] T. Nakamura, J. Phys. Soc. Jpn. **72**, 789 (2003).

[39] T. Nakamura, Phys. Rev. B **71**, 144401 (2005).

[40] L. A. Fernández and V. Martín-Mayor, Phys. Rev. B **91**, 174202 (2015).

[41] M. Lulli, G. Parisi, and A. Pelissetto, Phys. Rev. E **93**, 032126 (2016).

[42] F. Cooper, B. Freedman, and D. Preston, Nucl. Phys. B **210**, 210 (1982).

[43] T. Nakamura, Phys. Rev. E **93**, 011301(R) (2016).

[44] C. M. Bishop, *Pattern Recognition and Machine Learning* (Springer, New York, 2006).

[45] K. Harada, Phys. Rev. E **84**, 056704 (2011).

[46] F. Belletti, M. Cotallo, A. Cruz, L. A. Fernández, A. Gordillo-Guerrero, M. Guidetti, A. Maiorano, F. Mantovani, E. Marinari, V. Martin-Mayor, A. M. Sudupe, D. Navarro, G. Parisi, S. Perez-Gaviro, J. J. Ruiz-Lorenzo, S. F. Schifano, D. Sciretti, A. Tarancon, R. Tripiccione, J. L. Velasco, and D. Yllanes, Phys. Rev. Lett. **101**, 157201 (2008).

[47] L. A. Fernandez, E. Marinari, V. Martin-Mayor, G. Parisi, and J. J. Ruiz-Lorenzo, J. Stat. Mech. (2018) 103301.

[48] M. Baity-Jesi, E. Calore, A. Cruz, L. A. Fernandez, J. M. Gil-Narvion, A. Gordillo-Guerrero, D. Iñiguez, A. Maiorano,

E. Marinari, V. Martin-Mayor, J. Moreno-Gordo, A. Muñoz-Sudupe, D. Navarro, G. Parisi, S. Perez-Gaviro, F. Ricci-Tersenghi, J. J. Ruiz-Lorenzo, S. F. Schifano, B. Seoane, A. Tarancon *et al.*, Phys. Rev. Lett. **120**, 267203 (2018).

[49] H. G. Katzgraber and I. A. Campbell, Phys. Rev. B **72**, 014462 (2005).

[50] E. Marinari, G. Parisi, F. Ricci-Tersenghi, and J. J. Ruiz-Lorenzo, J. Phys. A: Math. Gen. **31**, 2611 (1998).

[51] J. Kisker, L. Santen, M. Schreckenberg, and H. Rieger, Phys. Rev. B **53**, 6418 (1996).

[52] T. Komori, H. Yoshino, and H. Takayama, J. Phys. Soc. Jpn. **69**, 1192 (2000).

[53] Y. G. Joh, R. Orbach, G. G. Wood, J. Hammann, and E. Vincent, Phys. Rev. Lett. **82**, 438 (1999).

[54] K. Hukushima and I. A. Campbell, arXiv:0903.5026v1.

[55] I. A. Campbell and D. C. M. C. Petit, J. Phys. Soc. Jpn. **79**, 011006 (2010).